

# The SNO+ Experiment

SNO+ Collaboration\*.<sup>†</sup>

The SNO+ experiment builds on the investment of capital and time by the Office Of Nuclear Physics in the Sudbury Neutrino Observatory (SNO) to create a broad physics program whose primary goal is a sensitive search for neutrinoless double beta decay. In five years of running LAB loaded with 0.3% by mass of natural Te, SNO+ will be able to set a limit on the lifetime for neutrinoless double beta decay of  $T_{1/2} > 9 \times 10^{25}$  years. The SNO+ collaboration has been able to load as much as 5% Te in LAB; a loading of 3% would provide a lifetime limit of  $T_{1/2} > 7 \times 10^{26}$  y in five years, corresponding to a limit on  $m_{\beta\beta} < 25$  meV if the IBM-2 nuclear matrix elements are used. The broader program of physics achievable by SNO+ includes studies of solar neutrinos with a goal of measuring the astrophysically interesting CNO neutrinos, reactor antineutrino oscillations, geoneutrinos, supernova neutrinos, and nucleon decay.

---

\* Submitting author Joshua Klein

<sup>†</sup>Electronic address: [jrk@hep.upenn.edu](mailto:jrk@hep.upenn.edu)

## I. EXECUTIVE SUMMARY

SNO+ is a multi-purpose neutrino experiment whose primary goal is a search for neutrinoless double beta decay ( $0\nu\beta\beta$ ) of  $^{130}\text{Te}$ . SNO+'s approach to  $0\nu\beta\beta$  is to load 0.3% by weight natural tellurium into linear alkyl benzene (LAB) liquid scintillator. The existing SNO detector, built with significant DOE investment, has been modified to counteract the buoyancy of the LAB-filled acrylic vessel (AV), and has been upgraded with new electronics and DAQ to handle the expected increase in data rate. The broader SNO+ program encompasses measurements of solar neutrinos including the astrophysically interesting CNO neutrinos, nucleon decay, reactor antineutrinos, geo-neutrinos, and observation of neutrinos from a supernova should one occur. The SNO+ Collaboration believes that this combination of broad physics program with the potential to reach the bottom of the  $0\nu\beta\beta$  inverted hierarchy region makes SNO+ a unique and compelling experiment. The possibilities for affordably scaling this approach even further are particularly exciting.

There are important advantages to the SNO+ approach to  $0\nu\beta\beta$  that allow a convincing discovery to be made. The great size of the detector means that external (“surface”) backgrounds can be eliminated via fiducialization while still retaining significant isotopic mass. The  $\beta\beta$  isotope and the detector are distinct, allowing us to make “target out” measurements before and after deployment. Measurements made before isotopic loading will allow us to measure many critical backgrounds, such as the activity of the LAB scintillator cocktail, the AV, and the PMT array, as well as allowing us to test our model of detector response. The liquid form of the detector volume also allows us to re-purify the Te and run again. The SNO+ Collaboration has already demonstrated that the purification technique reduces known cosmogenics (such as  $^{60}\text{Co}$ ) by factors of 100-1000 for each purification pass. Thus a false  $0\nu$  peak would need to be caused by an unknown, long-lived isotope that is entirely immune to our (very generic) recrystallization purification process. SNO+'s program of R&D and simulation has shown that, like BOREXINO and KamLAND, the fast timing of scintillation light means that many remaining backgrounds (such as internal  $^{214}\text{Bi}$ ) can be significantly reduced through  $\beta$ - $\alpha$  coincidence cuts. Multi-site  $\gamma$  or  $\beta$ - $\gamma$  events (e.g.,  $^{60}\text{Co}$ ) can be constrained by using the broader profile of their reconstructed PMT time residuals. Lastly, in the event that a signal appears real and large, SNO+ could deploy a second isotope with a different endpoint (such as  $^{150}\text{Nd}$ ) to determine whether a signal is seen there as well.

Our vision for SNO+ as a  $0\nu\beta\beta$  experiment goes well beyond this initial 0.3% loading phase. The pace of R&D in our approach to  $0\nu\beta\beta$  decay has been dramatic: in roughly two years the idea of loading Te has gone from a concept to the point where 5% loadings have been demonstrated. New purification techniques for and resultant purity levels of the various components in the Te-loaded scintillator cocktail have been developed and demonstrated, and the optical properties of the cocktail have been significantly improved.

A 3% loading of natural Te would correspond to roughly 2 tonnes of  $^{130}\text{Te}$  within our anticipated fiducial volume. To maintain the light yield necessary to do a tonne-scale  $0\nu\beta\beta$  search with this higher loading, we would replace and expand the coverage of the twenty-year-old PMT array with modern high-quantum efficiency tubes. Such an upgrade would still be inexpensive because it would leverage so much of the infrastructure already built for SNO+. Increasing the loading in SNO+ has the great advantage that many of the backgrounds *do not* scale with isotopic mass; thus lifetime sensitivity grows in nearly direct proportion to the total amount of Te.

We have developed a complete optical model of our Te-loaded scintillator cocktail based on measurements of bulk optical properties. With this model and our well-calibrated simulation of the detector response, we predict a light yield of 200 pe/MeV. With changes to the wavelength shifter (replacing bis-MSB with perylene), our measurements indicate we would get even higher yields, up to 300 pe/MeV. With off-the-shelf high quantum efficiency PMTs, this light yield would rise to roughly 600 pe/MeV, and full photocathode coverage could nearly double even that yield, resulting in an energy resolution at the  $0\nu$  endpoint of under 2%. With the conservative 200 pe/MeV light yield used for the 0.3% Te-loading sensitivities presented here, the optimal ROI is asymmetric, from  $-0.5\sigma$  to  $+1.5\sigma$ , centered on the  $0\nu$  endpoint. This ROI reduces the  $2\nu$  background by more than an order of magnitude with a signal loss of just 38%.

In this asymmetric ROI, the dominant background is  $^8\text{B}$  neutrinos (7.3 events/year). The low  $2\nu$  rate of Te leads to a leakage of just 2.1 events/year in the ROI, and fewer if perylene is used as the wavelength shifter. Our other background requirements all flow down from the need for them to contribute less than these two sources. We have calculated the production of cosmogenics on the Te before purification and have measured purification factors with spike sources. We have also assayed all components of the scintillator cocktail, and have run complete simulations and analyses of all backgrounds including “external” backgrounds created by  $\gamma$ -rays. These studies predict a total background in the ROI, including a fiducial volume restriction of  $R < 3.5$  m, of 18.6 events/year.

With a 0.3% loading, we therefore anticipate being able to set a 90% CL lifetime limit of  $T_{1/2} > 9 \times 10^{25}$  y in 5 years of running, corresponding to a limit  $m_{\beta\beta} < 67$  meV using the IBM-2 nuclear matrix elements [1, 2]. For a 3% loading, assuming we maintain the same light yield through an upgrade to the PMT array and the use of perylene, this limit goes up to  $T_{1/2} > 7 \times 10^{26}$  y, corresponding to a 90% limit on  $m_{\beta\beta} < 25$  meV in five years of running.

## II. SNO+ DETECTOR

The SNO+ detector will make use of infrastructure from the Sudbury Neutrino Observatory (SNO), located 2 km underground in the SNOLAB scientific laboratory in Sudbury, Canada. SNOLAB has an overburden of over 6 km water equivalent, resulting in a muon flux of just  $0.2 \mu/\text{m}^2/\text{day}$ . SNO's heavy water target will be replaced in SNO+ by 780 tonnes of linear alkyl benzene (LAB) liquid scintillator to study a large variety of fundamental neutrino physics. As Figure 1 shows, the inner volume consists of a 12-m diameter spherical acrylic vessel (AV) with a shell thickness of 5.5 cm. Approximately 9000 inward-pointed photomultiplier tubes (PMTs) with low-activity glass are mounted on a concentric geodesic structure, with the front faces of the PMTs at a mean distance of 8.35 m from the center of the detector.

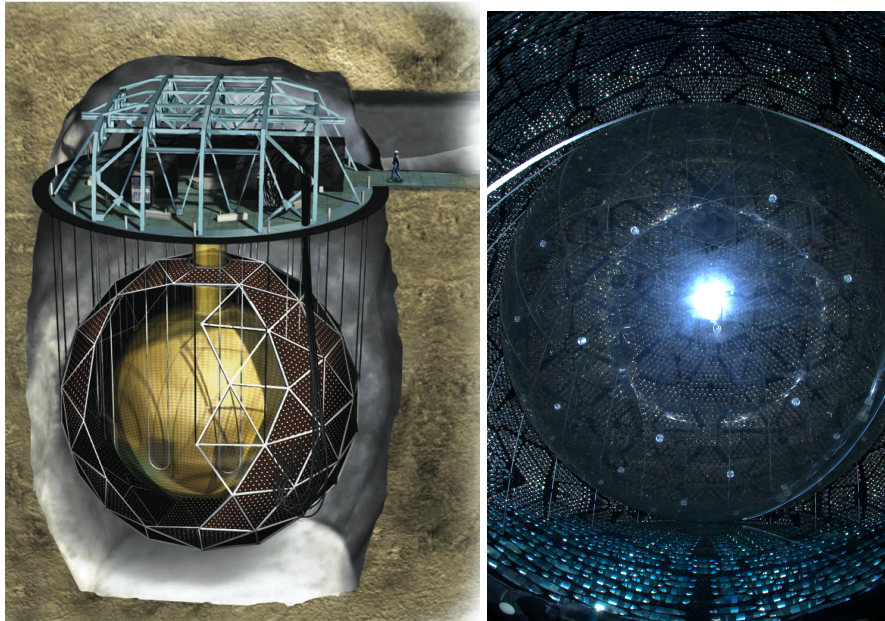


FIG. 1: Left: The SNO+ detector. The outer 18 m diameter geodesic structure holds  $\sim 9000$  inward-facing PMTs within a volume of highly purified water. LAB scintillator will fill the inner 12 m diameter acrylic vessel (AV). Right: A tensylon rope net has been installed around the AV to offset the buoyancy of liquid scintillator, and the initial water fill has started.

The volume external to the AV will be filled with ultra-pure water, providing several meters of shielding between the AV and external radiation from the PMT structure and cavity walls. A low-activity rope net placed over the upper part of the AV and attached to the cavity floor is used to offset the buoyant forces of the scintillator volume.

A number of additional significant upgrades have been made to the original SNO detector itself, including an improved cover-gas system, a new interface port for deploying calibration sources, upgrades to the data acquisition electronics for the higher rates of scintillator events, an embedded fiber-optic calibration system, a updated source deployment and retrieval mechanism, a new scintillator processing plant, and an upgraded water purification system.

The SNO+ LAB includes 2,5-diphenyloxazole (PPO) as the primary fluor. A method has been developed for loading tellurium into this mixture by dissolving telluric acid in water and using an amine-based surfactant to form a micro-emulsion. Good light transmission in the sensitive wavelength range for the PMTs has been achieved with minimal scattering. Loading as high as several percent of natural tellurium by weight has been achieved and the stability of the Te-loaded scintillator (TeLS) has been explicitly demonstrated on a timescale in excess of one year, over which time no noticeable degradation in optical properties has been observed. Figure 2 shows the relative absorption as a function of wavelength for the current “base” formulation of scintillator loaded with 0.3% (by weight) of tellurium. A tail of absorption extends to  $\sim 420$  nm, above which the mixture shows excellent transmission properties. Above  $\sim 440$  nm, we find that the transmission appears virtually indistinguishable from that of unloaded scintillator. As a consequence, a secondary fluor such as bis-MSB can be employed for the TeLS to shift the emission spectrum beyond the absorption tail, further boosting light transmission. We have also begun studies of using perylene as a secondary fluor. Perylene shifts the light to even longer wavelengths, getting well above the absorption of the scintillator.

We have measured the bulk optical properties of the complete Te-loaded scintillator cocktail, including absorption and re-emission, scattering, and intrinsic light yield. With these measurements, and with our detailed model of the

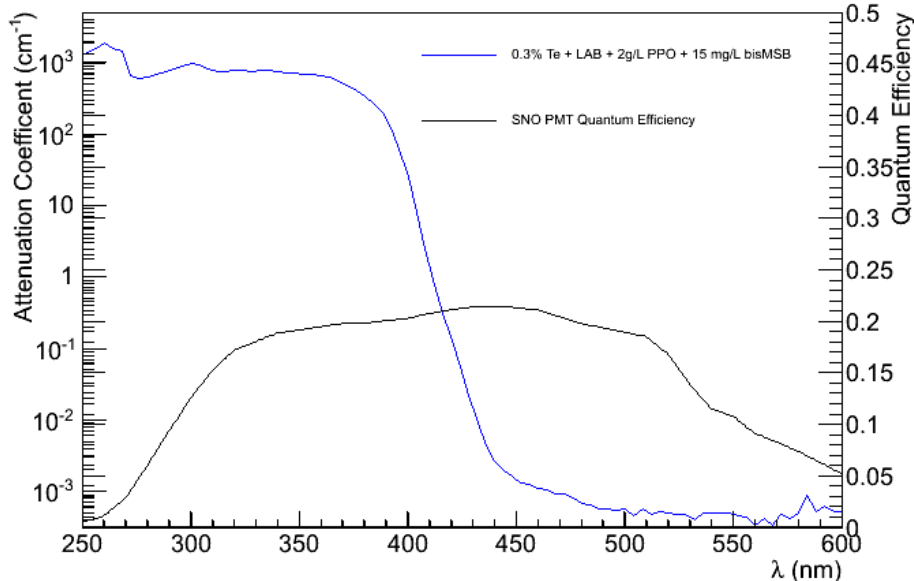


FIG. 2: Absorbance of Te-loaded LAB versus wavelength, with the SNO PMT quantum efficiency curves superimposed.

SNO+ geometry, we have created a complete hit-level Monte Carlo simulation (“RAT”). We have tested the simulation by comparing to data from SNO, and have found that it reproduces the detector response to better than 1%. With our measurements and model of the TeLS, the simulation predicts a detected light yield of 200 pe/MeV averaged over the detector volume. With perylene, the model predicts a light yield of up to 300 pe/MeV and, encouragingly, the longer wavelength light is less absorbed by additional Te. Thus with perylene, very high loadings may be possible.

### III. DOUBLE BETA DECAY

#### A. Backgrounds

For the purposes of our background estimation, we define an energy region-of-interest (ROI) that extends from roughly  $-0.5\sigma$  to  $1.5\sigma$  around the  $0\nu\beta\beta$  endpoint. Such an asymmetric ROI reduces the contributions from both the  $2\nu\beta\beta$  continuum and other low-energy backgrounds, but retains a large fraction of the expected  $0\nu\beta\beta$  signal region. We also choose a restrictive fiducial volume, excluding all events that reconstruct with a radial position beyond 3.5 m. With this fiducial volume restriction, we accept 20% of the total  $^{130}\text{Te}$  decays.

We divide the sources of background events in the ROI into a few major classes:

- *Cosmogenic Backgrounds*: Cosmogenically activated isotopes within the Te, created before the material is brought underground, can decay with energies that leak into the ROI.
- *External Backgrounds*:  $\gamma$ -rays caused by the decays of uranium- and thorium-chain radioactivity in the acrylic vessel, light water shield, and PMT array, that travel into the fiducial volume.
- $2\nu\beta\beta$ :  $\beta\beta$  events associated with the  $\nu\nu\beta\beta$  decay of  $^{130}\text{Te}$  which leak into the ROI due to finite energy resolution.
- $^8\text{B } \nu$ : Elastically scattered electrons from  $^8\text{B}$  neutrino interactions.
- *Internal U and Th chain*: Decays of uranium- and thorium-chain isotopes within the Te-loaded scintillator cocktail, that lead to visible energies near the  $2\nu\beta\beta$  endpoint.
- $(\alpha, n)\gamma$ : Neutrons created by  $(\alpha, n)$  reactions that capture on hydrogen and release a single 2.2 MeV  $\gamma$ , which then leak into the ROI due to finite energy resolution.

For each of these backgrounds, we predict the fraction that falls within the ROI and fiducial volume using the full SNO+ Monte Carlo simulation (RAT), with all reconstruction and analysis cuts applied. A complete model of the detector and scintillator optics is simulated, including the emission spectrum of LAB, the emission and re-emission spectra of the wavelength shifters (PPO and bis-MSB), the absorption and scattering lengths of all materials in the scintillator cocktail (including the Te, H<sub>2</sub>O, and surfactant), and a measurement of the intrinsic light yield in photons/MeV of the full cocktail. We have verified that the simulation reproduces the response of the SNO water Cherenkov detector to within 1%, and thus the simulation of the photomultiplier tubes, optics of the acrylic vessel and water shield, and electronics are known to be very accurate. We have also verified the approximate background numbers to a good accuracy using analytical models.

Our mitigation strategy has four critical components: purification of all materials and in particular the scintillator cocktail and isotope; the energy ROI window; the fiducial volume restriction; and finally timing-based tags and cuts that exploit  $\beta$ - $\alpha$  coincidences and the broadening of PMT hit time distributions for multi-site events. We discuss these in the context of each background below.

### 1. Cosmogenic Backgrounds

The decay of isotopes produced by the bombardment of natural tellurium by cosmogenic neutrons and protons at sea level can yield events within the ROI. Mitigation by purification and underground cooldown of the Te isotope is therefore critical. Isotopes that are dangerous for SNO+ have a decay end-point above 2 MeV, a half-life larger than 20 days, and a mass number smaller than <sup>131</sup>I. A total of 21 nuclides have been identified that satisfy these criteria: <sup>22</sup>Na, <sup>26</sup>Al, <sup>42</sup>Ar, <sup>44</sup>Ti, <sup>46</sup>Sc, <sup>56</sup>Co, <sup>58</sup>Co, <sup>60</sup>Fe, <sup>60</sup>Co, <sup>68</sup>Ge, <sup>82</sup>Sr, <sup>84</sup>Rb, <sup>88</sup>Y, <sup>88</sup>Zr, <sup>90</sup>Sr, <sup>102</sup>Rh, <sup>102m</sup>Rh, <sup>106</sup>Ru, <sup>110m</sup>Ag, <sup>124</sup>Sb and <sup>126</sup>Sn. These nuclides can give a direct contribution to the background level in the ROI, or can feed shorter-lived isotopes that are a direct background in the ROI.

The production rates of all the listed nuclides have been calculated [4] using the ACTIVIA code [5] and the neutron and proton fluxes at sea level parameterized by Armstrong [6][7] (total flux above 20 MeV of  $1.5 \times 10^{-3} n/s/cm^2$ ). The ACTIVIA program uses the cross sections obtained by the semi-empirical formulas described in Ref. [8][9][10]. Semi-empirical formulas were obtained for a proton flux and are generally valid for  $E > 100$  MeV. At high energy, the production cross sections for neutrons and protons are very close, and we therefore use the same equations. Our energy range for these calculations is 200 MeV - 100 GeV, with a step size of 10 MeV. For energies below 200 MeV, the neutron and proton cross sections are quite different [11]. We therefore use the TENDL-2009 [13] cross section database for neutrons and protons in the energy range from 10 MeV to 200 MeV together with the Armstrong cosmic flux parametrization to calculate the production rates. When relevant information was not available in the database, we used the ACTIVIA code in a nearby energy range, 100 MeV - 200 MeV. The resulting calculated production rates in  $\mu\text{Bq/kg}$  of natural tellurium are shown in Table I. Where relevant, the activities for parent isotopes are shown in brackets. As a check of our calculated production rates, the YIELDX routine [10] has also been used to calculate cross sections, and we find reasonable agreement.

Isotope	$T_{1/2}$ (d)	Q-value (MeV)	R ( $\mu\text{Bq/kg}$ )
<sup>44</sup> Sc (via <sup>44</sup> Ti)	0.17 (2.16E4)	3.65	1.19 (0.052)
<sup>46</sup> Sc	83.79	2.37	1.97
<sup>60</sup> Co (+ via <sup>60</sup> Fe)	1925.27 (5.48E8)	2.82	0.81 (0.367)
<sup>68</sup> Ga (+ via <sup>68</sup> Ge)	0.047 (271)	2.92	3.14 (1.28)
<sup>26</sup> Al	2.62E+8	4.00	0.67
<sup>82</sup> Rb (via <sup>82</sup> Sr)	8.75E-4 (25.35)	4.40	(2.44)
<sup>88</sup> Y (+ via <sup>88</sup> Zr)	106.63 (83.4)	3.62	3.14 (8.11)
<sup>42</sup> K (via <sup>42</sup> Ar)	0.51 (1.2E4)	3.53	1.33 (0.24)
<sup>56</sup> Co	77.2	4.57	0.13
<sup>58</sup> Co	70.9	2.31	1.29
<sup>110m</sup> Ag	249.83	3.01	2.39
<sup>110</sup> Ag (via <sup>110m</sup> Ag)	2.85E-4	2.89	(0.03)
<sup>106</sup> Rh (via <sup>106</sup> Ru)	3.47E-4 (371.8)	3.54	(0.06)
<sup>126m</sup> Sb (+ via <sup>126</sup> Sn)	0.01 (8.4E7)	3.69	71.42 (7.91)
<sup>126m</sup> Sb (+ via <sup>126m</sup> Sb)	12.35 (0.01)	3.67	89.65
<sup>22</sup> Na	950.6	2.84	1.01
<sup>84</sup> Rb	32.8	2.69	1.29
<sup>90</sup> Y (via <sup>90</sup> Sr)	2.67 (1.05E4)	2.28	0.69 (0.165)
<sup>102</sup> Rh (+ via <sup>102m</sup> Rh)	207.3	2.32	11.77 (0.03)
<sup>102m</sup> Rh	1366.04	2.46	11.77
<sup>124</sup> Sb	60.2	2.90	182

TABLE I: Calculated cosmogenic isotope production rates.

With our calculated radioactivity levels (assuming a full year of exposure at surface), cooldown alone is not enough to satisfactorily reduce the number of events that could contaminate the ROI. To remove these cosmogenic isotopes, a purification procedure using chemical-induced recrystallization has been developed at Brookhaven National Laboratory (BNL). The process is unique to our telluric acid compound but very generic in how it eliminates contaminants. The process has been shown to reduce the level of relevant contaminants by factors of several hundred or more per pass, allowing for the design of a large scale multi-pass system to meet our requirements. Table II shows the results of “spike” tests, in which the purification procedure was tested on Te samples that were contaminated with known quantities of various elements corresponding to the relevant cosmogenic isotopes.

Element	Reduction Factor	Assay Technique
Stage 1 Te purification, single-pass spike test		
Co	1492± 326	X-ray fluorescence
Sb	>243	
Sn	> 167	Auto-titration
Fe	> 100	X-ray fluorescence
Na	346	Auto-titration
Sc	> 165	X-ray fluorescence
Ge	> 333	X-ray fluorescence
Y	> 278	X-ray fluorescence
Zr	> 278	Auto-titration
Ag	> 278	X-ray fluorescence
Bi	348± 81	Th-228 tracer
Ra	397± 20	Th-228 tracer
Th	390±19	Th-228 tracer
Stage 1 Te purification, double-pass spike test		
Co	$3.7 \times 10^5$	X-ray fluorescence
Th		
Stage 2 (UG) Te purification, single-pass spike test		
Co	12	
Ag	> 20	
Zr	17	

TABLE II: Implied contaminant reduction factors from spike tests, and assay technique used to determine them.

We have shown through measurements that a second pass of the recrystallization process is nearly as efficient as the first pass, and thus we plan two purification passes, separated by less than three hours, followed by transport of the Te underground within 5 hours of the final pass. For logistical reasons, this “Stage I” purification process will take place in the SNOLAB surface building, and because of the small re-activation that will occur as the result of surface exposure during this process, a less efficient but simpler secondary system has been developed that is better-suited for purification underground. The underground “Stage II” purification, using thermally-induced recrystallization, will perform two additional passes to reduce contaminants by more than a factor of 100. A further 3-6 months of “cooling” underground is anticipated to then allow any remaining short-lived isotopes (which are the ones most likely to be produced by surface exposure during Stage I) to decay to negligible levels.

## 2. External backgrounds

The vast majority of radioactive backgrounds from external sources are due to  $^{208}\text{Tl}$  and  $^{214}\text{Bi}$  arising from the  $^{232}\text{Th}$  and  $^{238}\text{U}$  contained in the SNO+ AV, light water shield, and PMT glass. In particular,  $^{232}\text{Th}$  has a half life of  $1.4 \times 10^{10}$  years, with the short-lived daughter isotope  $^{208}\text{Tl}$  ( $t_{1/2} = 3$  minutes, BR=36%) being of primary concern.  $^{208}\text{Tl}$  undergoes  $\beta$  decay to one of the excited states of  $^{208}\text{Pb}$ , which then decays to the ground state by emission of a 2.614 MeV  $\gamma$ . Although the Q-value of the  $^{208}\text{Tl}$  decay is 4.99 MeV, the 2.614 MeV gamma can occasionally travel long distances into the detector on its own, with the other decay products undetected, so as to deposit energy within the ROI. Some background is also contributed from the  $^{238}\text{U}$  chain via the short lived isotope  $^{214}\text{Bi}$  ( $t_{1/2} = 19.9$  minutes) and the subsequent decays by beta and gamma emission with a Q-value of 3.27 MeV. However, the contribution to the ROI from this is noticeably less than from the  $^{208}\text{Tl}$  decays. The various sources of external backgrounds with radiopurity estimates and yearly decay rates are summarized in Table III.

We have simulated background events from each of these sources, as shown in Figure 3, which shows the radial distributions of external events in terms of the normalized cubic radius,  $(R/R_{AV})^3$ , with no energy ROI cut applied. We find as expected that contributions from the sources nearest the scintillator (the AV and hold-down rope net)

Source	Mass	Isotope	Activity	Decays/year
Internal ropes	45.2 g	$^{214}\text{Bi}$	$2.8 \times 10^{-10} \text{ gU/g}$	4966
		$^{208}\text{Tl}$	$2.0 \times 10^{-10} \text{ gTh/g}$	418
Hold-down ropes	222.09 kg	$^{214}\text{Bi}$	$0.58 \pm 0.40 \text{ Bq/kg}$	$4.06 \times 10^6$
		$^{208}\text{Tl}$	$0.33 \pm 0.17 \text{ Bq/kg}$	$2.3 \times 10^6$
Water Shielding	1555 t	$^{214}\text{Bi}$	$2.1 \times 10^{-13} \text{ gU/g}$	$1.26 \times 10^8$
		$^{208}\text{Tl}$	$5.2 \times 10^{-14} \text{ gTh/g}$	$3.73 \times 10^6$
Acrylic Vessel (AV)	30 t	$^{214}\text{Bi}$	$1.0 \times 10^{-12} \text{ gU/g}$	$1.18 \times 10^7$
		$^{208}\text{Tl}$	$1.0 \times 10^{-12} \text{ gTh/g}$	$1.39 \times 10^6$
AV Dust (External)	$0.1\text{-}0.6 \mu\text{g/cm}^2$ <sup>a</sup>	$^{214}\text{Bi}$	$1.1 \times 10^{-6} \text{ gU/g}$	$7.8 \times 10^5$
		$^{208}\text{Tl}$	$5.6 \times 10^{-5} \text{ gTh/g}$	$4.6 \times 10^5$
AV Dust (Internal)	$0.02 \mu\text{g/cm}^2$	$^{214}\text{Bi}$	$1.1 \times 10^{-6} \text{ gU/g}$	$4.15 \times 10^4$
		$^{208}\text{Tl}$	$5.6 \times 10^{-6} \text{ gTh/g}$	$2.48 \times 10^4$
PMTs	9456 PMTs	$^{238}\text{U}$	$100 \mu\text{g/PMT}$	$3.7 \times 10^{11}$
		$^{232}\text{Th}$	$100 \mu\text{g/PMT}$	$4.4 \times 10^{10}$

<sup>a</sup> $0.1 \mu\text{g/cm}^2$  is the target background level, but  $0.6 \mu\text{g/cm}^2$  is the measured average dust concentration before cleaning the AV. It is assumed that the bottom half of the AV is at target level and the top half is uncleaned.

TABLE III: Summary of sources of external backgrounds, with estimated radioactivity and yearly number of decays. The last column gives the expected number of events/year within the full scintillator volume and across the entire energy spectrum.

dominate the leakage into the fiducial volume. These have a combined estimated activity equivalent to  $\sim 4 \times 10^6$

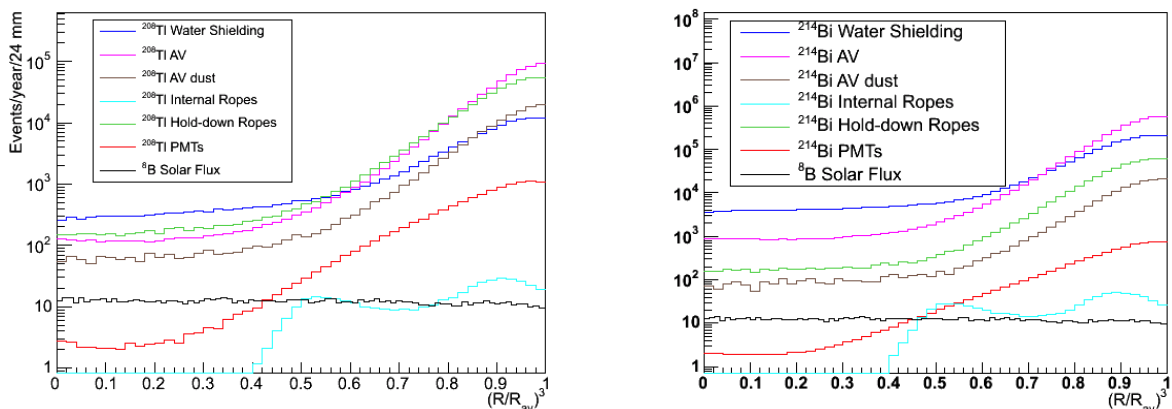


FIG. 3: Left: Normalized cubic radial distribution  $(R/R_{AV})^3$  for external  $^{208}\text{Tl}$  events from various sources within the SNO+ detector, with no energy ROI cut applied. For comparison, the background levels from  $^8\text{B}$  are shown. Right: Same distribution for  $^{214}\text{Bi}$  events.

decays of  $^{208}\text{Tl}$  per year. With a radial restriction for signal events of  $R < 3.5$  m, however, the fiducial mass is over 2.5 m from even these nearest background sources, roughly ten times the 26.3 cm Compton scattering length. Combined with the solid angle acceptance for gammas to reach this volume, the fraction of such events that can appear in the signal ROI is greatly reduced. In addition to the fiducial volume restriction, we have also developed cuts that reject events whose PMT hit time distributions are inconsistent with single-site energy deposits, reducing external background events that fall within the fiducial volume by roughly a factor of two. With the fiducial volume cut and the PMT timing cuts, we find a total of just 3.4 events per year from all external sources fall within our energy ROI.

### 3. Internal U/Th Backgrounds

Unlike external backgrounds, radioactive decays within the fiducial volume itself cannot be removed by fiducialization. The dominant source of such internal backgrounds are from uranium and thorium chain radioactivity. There are fortunately only a few sources of these: the scintillator cocktail which includes the LAB scintillator, wavelength-

shifters, surfactant, and water, and the Te isotope. Purification—and re-purification if necessary—of these materials is our primary mitigation strategy, but for some of the most troublesome sources we have coincidence tags and timing cuts that significantly reduce their levels.

It has previously been demonstrated by the BOREXINO collaboration [3] that it is possible to achieve very low levels of uranium and thorium in organic liquid scintillator, at the level of  $\sim 10^{-17}$ g/g. We assume for our background estimates that SNO+ will achieve the same purity levels in our LAB and associated wavelength shifters (PPO and bis-MSB) as was achieved by BOREXINO for its scintillator.

For the uranium and thorium levels in the  $\text{H}_2\text{O}$  that is used to load the Te, we assume we will achieve levels that are the average of the SNO collaboration's  $\text{H}_2\text{O}$  and  $\text{D}_2\text{O}$  purity levels, or  $3.5 \times 10^{-14}$ g/g for U, and  $3.5 \times 10^{-15}$ g/g for Th. Preliminary measurements of the water purity in the current SNO+ water plant show that levels are somewhat better than this, but we conservatively assume we will do no better than this target.

Our target levels for the surfactant used to load the Te is the same as that for the associated  $\text{H}_2\text{O}$ . We have measured the starting U and Th levels in the surfactant using ICP-MS, and find limits at  $1 \times 10^{-11}$ g/g and  $1 \times 10^{-12}$ g/g respectively. Using a metal scavenger (QuadraSil), we have been able to show reductions on the benchtop of  $10^5$  for U and  $4 \times 10^5$  for Th, which puts us well below our target levels. Nevertheless, we again assume we will only reach purity levels consistent with our targets.

For the Te itself, we have used ICP-MS to measure initial levels of U and Th contamination, finding limits of  $2.3 \times 10^{-11}$ g/g and  $2.8 \times 10^{-11}$ g/g respectively. The multi-pass recrystallization procedure described in Section III A 1 will be used to remove U and Th contamination. We have found that, like the cosmogenic isotopes of Section III A 1, the recrystallization procedure reduces backgrounds by factors of  $10^5$  after two passes, bringing our expected levels comfortably below our targets.

The principle U chain decays that directly contribute to the ROI are  $^{214}\text{Bi} \rightarrow ^{214}\text{Po}$  (Q-value=3270 keV,  $\beta^-$ -decays with BR=99.979%). These decays can be very efficiently identified by the delayed 7.7 MeV  $\alpha$  emitted by the subsequent decay of  $^{214}\text{Po}$  ( $t_{1/2}=164 \mu\text{s}$ ) to  $^{210}\text{Pb}$ . We remove these events in two ways. For decays in which the  $\alpha$  occurs more than  $\sim 250$  ns after the  $\beta$ , the SNO+ detector will record them as distinct events, with the  $\alpha$  event having a visible energy of roughly 800 keV, well above the anticipated SNO+ energy threshold. Therefore removing all events in the ROI for which a second triggered event is within 1.3 ms (eight lifetimes) eliminates 99.8% of  $^{214}\text{Bi} \rightarrow ^{214}\text{Po}$  in which the  $\beta$  falls within the ROI. Such a long time window, naively applied, could eliminate signal acceptance due to accidental coincidences between a putative  $0\nu$  event and some other background event. We retain significant signal acceptance by also requiring the second event to fall within a very broad energy window centered on the  $\alpha$  energy and within a meter or so of the primary  $\beta$ . For events in which the  $\alpha$  decay occurs within 250 ns of the  $\beta$ , we use the PMT hit times in the single event window to reject the event. In practice, this is done by fitting the PMT hit time residuals under both the hypothesis that the event is a  $\beta\beta$  event and the hypothesis that it is a  $\beta\alpha$  event, and comparing the likelihoods. This rejects such events by another factor of 50, for a total rejection of 1/25000.

Another route for the  $^{214}\text{Bi}$  decay to  $^{210}\text{Pb}$  is via  $^{210}\text{Tl}$ , which occurs with a branching fraction of 0.021%. In this case, a 5.5 MeV alpha from the first step precedes the subsequent decay of  $^{210}\text{Tl}$  (Q=5.49 MeV, half-life = 1.3 minutes). The small branching fraction means that the requirements for rejecting these events are far less stringent than for the dominant  $^{214}\text{Bi}$ - $^{214}\text{Po}$  decays. While we anticipate being able to remove some fraction by looking for  $\alpha$ -like events followed by a  $\beta$  event a small distance away, we conservatively assume no rejection beyond the ROI restriction for these events.

For the Th chain, the decay sequence  $^{212}\text{Bi} \rightarrow ^{212}\text{Po} \rightarrow ^{208}\text{Pb}$  can also contribute the background in the ROI. The first decay is a  $\beta$  with an endpoint of 2.252MeV, and the second an  $\alpha$  with energy  $E_\alpha = 8.78\text{MeV}$  and a half-life of  $\tau_{1/2} = 300$  ns. When the  $\alpha$  follows promptly, its visible energy of roughly 900 keV can pile up with the preceding  $\beta$  and leak into the ROI. We remove these events in the same way as piled-up  $\beta\alpha$  events from the decay of  $^{214}\text{Bi}$  are rejected, via hypothesis tests on the PMT time residuals. Our analyses of simulated events show that we can reject these events 98% of the time (and for the roughly 50% of the decays that create distinct SNO+ triggered events, a  $\beta$  followed by an  $\alpha$ , we easily reject all of them with the same coincidence cut used for  $^{214}\text{Bi}$ ). Additional rejection of this background that makes use of correlated decays occurring earlier in the Th chain may also be possible depending on the thermal stability of the detector, which could permit “look-back times” of several hours or more. We do not include such long lookback-time reductions in our analysis here.

There is a second decay path for  $^{212}\text{Bi}$ ,  $^{212}\text{Bi} \rightarrow ^{208}\text{Tl} \rightarrow ^{208}\text{Pb}$ , with a branching ratio of 36%. The first decay proceeds via the emission of an  $\alpha$  of energy 6 MeV (visible energy  $\sim 600$  keV), and the second via  $\beta$  and  $\gamma$  emission with a half-life of 3.1 minutes. Because of their high summed energy, only a small fraction of these  $^{208}\text{Tl}$  decays can leak into the ROI.

Lastly, at the tops of the two chains there is  $^{234m}\text{Pa}$  (U) and  $^{228}\text{Ac}$  (Th) which can both decay via  $\beta$  emission, and produce events that can leak into the ROI from below. Our asymmetric ROI helps reduce these significantly.

Combining our assumptions about LAB purification, our measurements of the purification levels of the surfactant and radioactivity of the water, and our measurements of the intrinsic radioactivity of the Te and our purification

factors via re-crystalization, we use our Monte Carlo simulation to generate events that look like anticipated SNO+ data. We then apply our position and energy reconstruction algorithms, as well as the cuts described above, to count the number of events that leak into our ROI. Table IV summarizes these backgrounds leakage numbers for internal sources.

Species	Mitigation	Counts/yr in ROI
<i>Uranium Chain</i>		
$^{234m}\text{Pa}$	Purification	0.05
$^{214}\text{Bi} - \text{Po}$	$\beta$ - $\alpha$ Coincidence	0.7
$^{210}\text{Tl}$	Purification	1.3
<i>Thorium Chain</i>		
$^{228}\text{Ac}$	Purification	1.0
$^{212}\text{Bi} - \text{Po}$	$\beta$ - $\alpha$ Coincidence	1.89
$^{208}\text{Tl}$	Delayed $\beta$	0.02
<i>Total Internal</i>		
<i>U-Th Chain Background</i>		5.0

TABLE IV: Sources of internal backgrounds, primary mitigation strategies, and expected number of events within the ROI.

#### 4. $(\alpha, n)\gamma$

Neutrons produced in the liquid scintillator (primarily via  $\alpha + {}^{13}\text{C} \rightarrow {}^{16}\text{O} + n$ ) are a potential background to  $0\nu\beta\beta$  in  ${}^{130}\text{Te}$  because the 2.2 MeV  $\gamma$ s created when they capture on hydrogen are not far below the  $0\nu$  peak energy, and because collisions with protons can produce events with a continuum of energies. Therefore  $\alpha$ s that do not themselves produce events within the ROI are still potentially dangerous.

As shown by the BOREXINO and CUORE experiments, a major source of  $\alpha$  decays is  ${}^{210}\text{Po}$  ( $E_{\alpha} = 5.3$  MeV). There are other  $\alpha$ s in the U and Th chain, with higher energies than those of  ${}^{210}\text{Po}$ , but their contributions are negligible compared to  ${}^{210}\text{Po}$ . For SNO+, the  ${}^{210}\text{Po}$  comes from both the Te isotope and from leaching of  ${}^{210}\text{Pb}$  from the acrylic vessel. We take as the fraction of  ${}^{210}\text{Po}$  added with the tellurium the measurements of the CUORE collaboration for the CCVR crystals [12]. The assumed activity is about 0.06 Bq/kg $_{\text{Te}}$ . The relatively short half-life of  ${}^{210}\text{Po}$  ( $T_{1/2} = 138.4$  d) means that in just one year this background is reduced to 16% of its initial rate. For the Po which comes from leaching off of the AV, we use our own measurements, including measurements of Pb leaching. We conservatively assume that any leached radioactivity distributes itself uniformly within the LAB volume, and with this assumption find that Po added with the Te and that leached from the AV contribute roughly equally in Year 1 to neutron production. In subsequent years, Po resulting from leaching increases as that added with the Te decays away and the load of leached  ${}^{210}\text{Pb}$  lead ( $T_{1/2} = 22.2$ yr) builds up.

In principle, some of these events can be removed by looking for the prompt  $\gamma$  or  $e^+e^-$  pairs created in the stripping reaction off of  ${}^{13}\text{C}$ , by looking for the prompt  $\alpha$  scintillation light created before the stripping reaction, and by looking for the light created by recoil protons as the neutron scatters before thermalization. We conservatively assume here no additional rejection by looking for these coincidences.

In Table V we list all sources of neutrons for the Te-loaded scintillator along with the expected number of events during the first year of data taking (Year 1) and in five years of measurement (5 Years).

Source	Year 1	5 Year Total
${}^{238}\text{U}$ spontaneous fission	0.9	4.5
$(\gamma, n)$	<0.1	<1
$\alpha + {}^{13}\text{C} \rightarrow {}^{16}\text{O} + n$	296	3195
$\alpha + {}^{18}\text{O} \rightarrow {}^{21}\text{Ne} + n$	3	30
$\alpha + {}^{17}\text{O} \rightarrow {}^{22}\text{Ne} + n$	0.2	3

TABLE V: Expected number of neutrons for the different neutron sources inside the scintillator. These are before any ROI or fiducial volume restriction.

## B. $0\nu\beta\beta$ Sensitivity

Table VI summarizes the background totals that fall within the fiducial volume and ROI discussed above in Section III A, plus the additional backgrounds from  $^8\text{B}$  neutrinos and the  $2\nu\beta\beta$  decay of  $^{130}\text{Te}$ . For the normalization of the  $2\nu\beta\beta$  background, we use the lifetime measured by the NEMO3 collaboration and, for the  $^8\text{B}$  background, we use global fits to the solar mixing parameters and total  $^8\text{B}$  flux [14].

Isotope	1 Year	5 Years
$2\nu\beta\beta$	2.1	10.5
$^8\text{B}$ $\nu$ ES	7.3	36.6
Uranium Chain	2.1	10.3
Thorium Chain	2.9	14.7
External	3.4	16.9
$(\alpha, n)$ 2.2 MeV $\gamma$	0.1	0.78
Cosmogenics	0.76	0.85
Total	18.6	90.6

TABLE VI: Expected total background counts in signal ROI in SNO+ for 1 and 5 live-years. The signal ROI is defined by a 3.5 m fiducial volume. The signal ROI is defined by a 3.5 m fiducial volume cut and an energy range [2.471, 2.699], corresponding to  $[\mu - \frac{1}{2}\sigma, \mu + \frac{3}{2}\sigma]$  of the Gaussian  $0\nu\beta\beta$  peak.

The expected number of  $0\nu\beta\beta$  decays occurring in the SNO+ detector is given by

$$S = \epsilon \cdot N_{130} \cdot \ln 2 \cdot \frac{t}{T_{1/2}^{0\nu\beta\beta}} \quad (1)$$

where  $\epsilon$  is the signal detection efficiency,  $N_{130}$  is the number of  $^{130}\text{Te}$  atoms in the detector,  $t$  is the live time, and  $T_{1/2}^{0\nu\beta\beta}$  is the half-life of  $^{130}\text{Te}$   $0\nu\beta\beta$ .

For our sensitivity estimate, we assume that our observed number of events is equal to the expected backgrounds from Table VI. We have set our limit using the method of Feldman and Cousins, though Bayesian estimates yield very similar results. Inverting Equation 1, we get for a five-year livetime a lower limit of  $T_{1/2}^{0\nu\beta\beta} > 9 \times 10^{25}$  y (90% C.L.) on the  $^{130}\text{Te}$   $0\nu\beta\beta$  half-life.

Figure 4 shows the expected  $2\nu$  and background spectra with an example  $0\nu$  peak with  $m_{\beta\beta} = 200$  meV shown, for our initial 0.3% loading. It is clear that knowledge of the energy scale and resolution are important. Yet for our asymmetric ROI, even a smearing of 5% on energy resolution only produces leakage from the  $2\nu$  continuum that is equal to the existing  $^8\text{B}$  background. Fitting the  $2\nu$  spectrum determines the energy resolution to 4%, even before calibration sources are deployed.

We constrain the background normalizations within the ROI using known values for some of the backgrounds ( $^8\text{B}$  and  $2\nu\beta\beta$ ) and fitting background levels in various sidebands. External backgrounds, for example, are very well determined (to better than a few percent) by fitting events outside the fiducial volume. Leakage of  $^{214}\text{Bi}$  and  $^{212}\text{Bi}$  events are likewise determined to better than 5% by counting events with easily tagged coincidences, and extrapolating inward to those in which the  $\beta$  and  $\alpha$  are separated by too small a time to be distinguished.

The only backgrounds not well-constrained by such sidebands are events from residual cosmogenics. While we expect our purification and cooldown to reduce these to negligible levels, we have nevertheless been able to show that the multi-site nature of such events (which typically included one or more  $\gamma$ s) provides some statistical discrimination from  $0\nu$  events. The multi-site events have broader time-of-flight-corrected PMT time residuals than to the single-site  $\beta\beta$  events. Using PDFs of the time residuals, we can calculate likelihood ratios for each event under the hypothesis that it is single-site or multi-site. Figure 5 compares these likelihood ratio distributions for  $\beta\beta$  events and  $^{60}\text{Co}$  events. While we cannot use such distributions to remove  $^{60}\text{Co}$  and other cosmogenics on an event-by-event basis, we nevertheless can fit any putative  $0\nu$  peak for the relative fractions of cosmogenics and  $0\nu$  events.

Figure 6 shows the SNO+ sensitivity for a 0.3% loading as a function of livetime, for both 90% CL limits and  $3\sigma$  detection levels.

Fortunately for this technique, as additional Te is added, the majority of the expected backgrounds do not change. The dominant  $^8\text{B}$  background is fixed, the external backgrounds from the AV and ropes also do not change, and the internal U and Th chain backgrounds associated with the LAB remain the same. With perylene as a wavelength shifter, and with an upgraded PMT array to include more coverage and high-quantum efficiency tubes, we calculate that we would have a light yield of 800 pe/MeV, before any losses due to the additional Te itself. We conservatively assume we reach just 300 pe/MeV for a loading of 3%. With this loading, we can expand the fiducial volume because

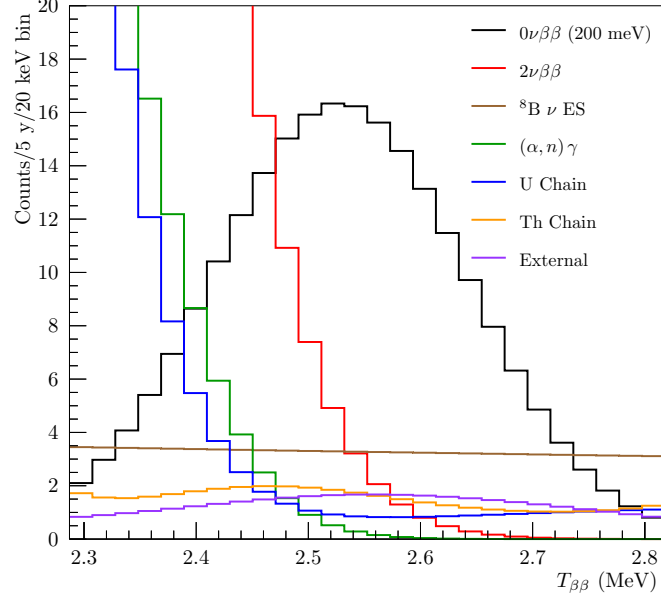


FIG. 4: Summary plot of all backgrounds and a hypothetical  $0\nu$  signal corresponding to a mass  $m_{\beta\beta} = 200$  meV.

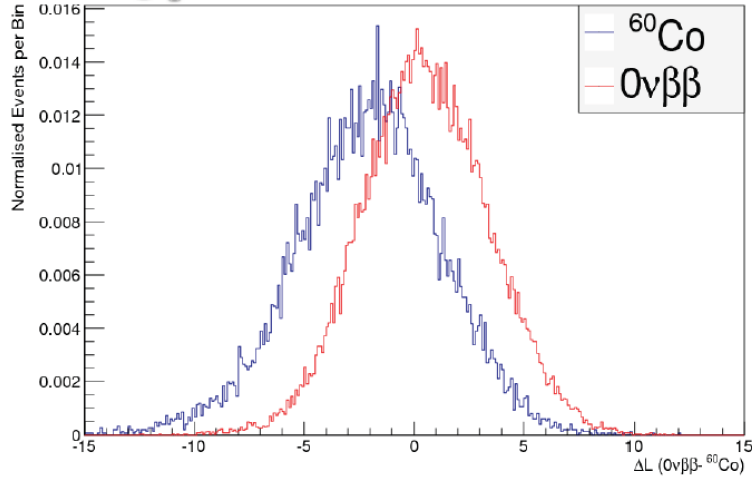


FIG. 5: Comparison of likelihood ratio distributions for  $\beta\beta$  events and  $^{60}\text{Co}$  events, each calculated under single-site and multi-site hypotheses.

the external backgrounds are now a relatively small fraction of the total. With these assumptions, a 3% loading would bring SNO+ to a 90% CL limit of  $T_{1/2} > 7 \times 10^{26}$  y, or, for the IBM-2 nuclear matrix elements, a limit of  $m_{\beta\beta} < 25$  meV.

## IV. OTHER PHYSICS WITH SNO+

### A. Solar Neutrinos

With solar neutrino flavor conversion clearly demonstrated by SNO, KamLAND, and other experiments, attention is turning toward more precision measurements in the solar sector. These measurements have implications for both

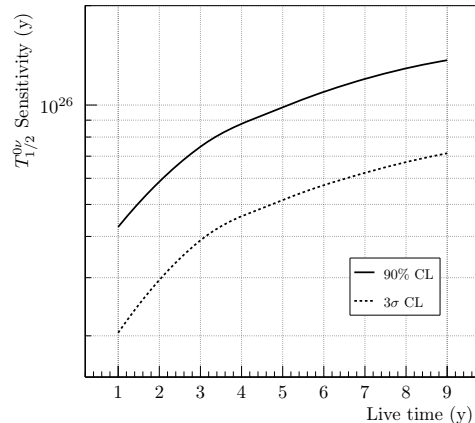


FIG. 6: Sensitivity versus livetime for SNO+  $0\nu\beta\beta$  search, for both 90% CL limits and  $3\sigma$  detection.

neutrino physics and solar astrophysics. A short low-energy SNO+ solar neutrino run will come during a short period before the Te is added. After the double beta decay search concludes, the Te will be removed and additional solar neutrino running can be done. For the higher-energy  ${}^8\text{B}$  solar neutrinos, much of the interesting physics can be done concurrent with the  $\beta\beta$  run.

The MSW or matter effect, which is the primary way in which long-baseline experiments plan to resolve the neutrino mass hierarchy, has to date only had a major impact on measurements of solar neutrinos. For solar neutrinos, one of the predictions of the MSW effect is a transition region between matter-enhanced and vacuum-dominated flavor transformation. The position and width of the transition region can be very sensitive to new physics: anything that changes the way in which neutrinos couple to matter can be resonantly enhanced and thus lead to dramatic shifts. Measurements in both the high-energy matter-enhanced region and the low-energy vacuum-dominated region have now been performed by several experiments, but none has yet observed neutrinos directly in the transition region itself. We therefore are left looking for data more deeply within the transition region that will constrain (or point toward) the new physics scenarios. Precision measurements of solar neutrino fluxes between 1 and 5 MeV—including the  ${}^8\text{B}$  and  $pep$  neutrinos—are therefore particularly interesting.

Other mysteries to be resolved include the solar surface metallicity. The Standard Solar Model (SSM) was always in excellent agreement with helioseismology, until recent measurements of the metallicity produced lower values, introducing a new discrepancy. Serenelli, Haxton, and Peña-Gray [16] have even speculated that perhaps the solar surface is metal poor because the gas giants actually swept out the metals toward the end of solar system formation. Accurate measurement of neutrino fluxes, in particular the CNO flux, could resolve this uncertainty, and therefore provide an interesting connection between solar system formation and neutrino physics.

SNO+’s great depth, its size, and the BOREXINO-inspired design of its scintillator plant all make it an excellent place to help answer these remaining solar neutrino questions. Our sensitivity to the lowest-energy  $pp$  solar neutrinos, recently directly observed by BOREXINO [15], will depend on the levels of  ${}^{14}\text{C}$  and  ${}^{85}\text{Kr}$  in the LAB. At the initial background levels of BOREXINO, we would reach a few percent uncertainty in a year of running. For the CNO neutrinos, the depth of SNO+ leads to very small cosmogenic  ${}^{11}\text{C}$ . With cuts like those used by BOREXINO, the backgrounds from  ${}^{11}\text{C}$  will become negligible, leaving only the levels of  ${}^{210}\text{Bi}$  as the critical issue. The  ${}^8\text{B}$  neutrinos will be easily visible at energies above the  ${}^{208}\text{Tl}$  decays. Figure 7 shows a fit to a full Monte Carlo simulation of all solar signals and backgrounds, and Table VII shows the resultant expected uncertainties on the various fluxes.

One final issue is the level of  ${}^{210}\text{Po}$  leaching from the acrylic vessel, as discussed above in Section III A. The SNO+ collaboration had initially planned on sanding the acrylic vessel to reduce these backgrounds, but deferred this in order to advance the SNO+ schedule. Nevertheless, we have been investigating an EDTA wash which, if viable, could be deployed during the water fill run that precedes the scintillator run. A five-month EDTA “soak” will reduce the amount of  ${}^{210}\text{Po}$  leaching into the LAB scintillator by roughly a factor of three.

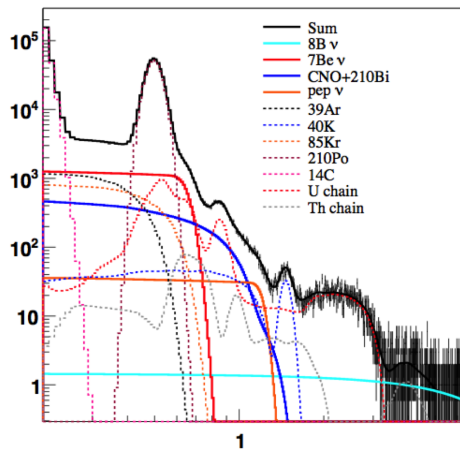


FIG. 7: Fit to Monte Carlo simulated solar neutrino events and backgrounds.

Source	1-year (stat)
$pep$	9.1%
${}^8\text{B}$	7.5%
${}^7\text{Be}$	4%
$pp$	$\sim 3\%$
CNO	$\sim 15\%$

TABLE VII: Expected statistical precision on solar neutrino flux measurements in SNO+ after one year of solar running. The  $pp$  precision depends on the intrinsic levels of  ${}^{14}\text{C}$ , which are at this time unknown, and the CNO precision depends on levels of  ${}^{210}\text{Bi}$ . We assume that BOREXINO purification techniques are successful in cleaning the LAB.

## B. Supernova Neutrinos

Like KamLAND, SNO+ will be sensitive to supernova  $\bar{\nu}_e$ s through inverse  $\beta$  decay on hydrogen, and to neutrinos and antineutrinos of all flavors through elastic scattering of electrons and other scattering processes that can proceed via neutral currents. One particularly interesting detection channel, however, will be the neutral current process  $\nu_x + p \rightarrow \nu_x + p$ , with scintillation light generated by the proton. As Figure 8 shows, to observe this reaction, we will need a low threshold—preferably below 200 keV of electron-equivalent visible energy—and hence the quenching of scintillation light for protons must be acceptably low. Using proton recoils from a neutron beam, measurements of LAB have shown us [17] that the quenching is acceptably low. Figure 9 shows the proton quenching and the resultant visible energy spectrum expected in SNO+. The electronics and DAQ upgrade to SNO+ will easily accommodate the data rate needed to observe these events, although to keep the overall data volume reasonably small we have developed a “Level 2” software trigger which will reduce the overall data volume. In addition, the SNO+ collaboration is working on an additional upgrade to the trigger system, which would allow “burst” triggering: essentially retaining buffered low-threshold events that are well below 200 keV for short periods of time, if it appears a supernova event burst is underway. We anticipate with a very conservative threshold of 200 keV that we would see roughly 100 events from the neutral current elastic scattering of protons, for the supernova shown in Figure 8.

## C. Nucleon Decay

SNO+ will perform searches for nucleon decay in both its initial water phase, and during its scintillator phase. During the water phase, SNO+ will be able to set a new limit on nucleon decay to undetected particles (e.g.,  $3\nu$ s). The signal is the subsequent emission of a  $\sim 6$  MeV  $\gamma$  from de-excitation of the residual nucleus. SNO+ has good sensitivity to these decays because of its great depth and cleanliness—the primary backgrounds are just solar neutrinos and reactor antineutrinos. SNO was limited in this measurement because the neutral current interaction by solar neutrinos led to a very high background, caused by the capture of neutrons on deuterons and the emission of a

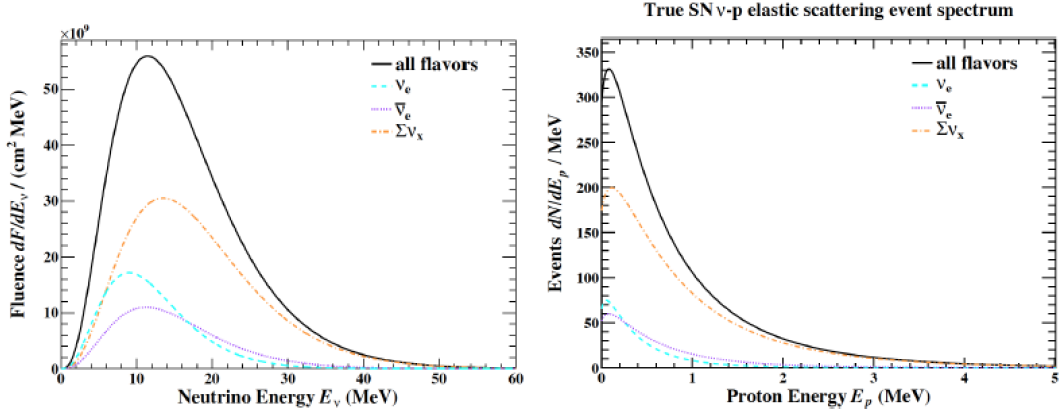


FIG. 8: Left: Spectrum of supernova neutrinos and antineutrinos of all flavors, observable by SNO+. Right: True energy spectrum of elastically scatter protons via neutral current interactions from supernova neutrinos, for a supernova at 10 kpc with a total neutrino energy of  $3 \times 10^{53}$  erg and mean energies of 12 MeV, 15 MeV and 18 MeV for  $\nu_e$ ,  $\bar{\nu}_e$ , and  $\nu_x$ , respectively.

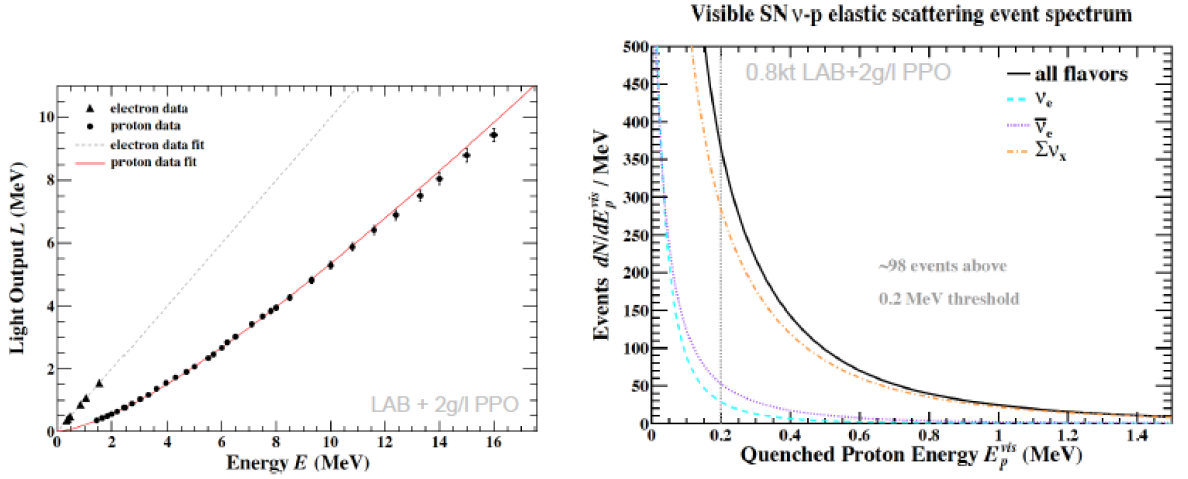


FIG. 9: From Ref. [17]. Left: Measurements of proton quenching from Ref. [17]. Right: Resultant visible energy spectrum of elastically scatter protons via neutral current interactions from supernova neutrinos.

6.25 MeV  $\gamma$  ray. With 6 months of water data, SNO+ can set a limit of  $8.2 \times 10^{30}$  yr and  $9.1 \times 10^{30}$  yr on decays of neutrons and protons respectively into invisible modes. These are an order of magnitude better than the current best limit of  $5.8 \times 10^{29}$  yr, set by KamLAND [18].

During its scintillator phase, SNO+ will have sensitivity to proton decays to the  $K^+\bar{\nu}$  mode. Work on analyses for this search are now underway.

#### D. Geo- and Reactor Antineutrinos

Like KamLAND and BOREXINO, SNO+ has sensitivity to both reactor antineutrinos and geoneutrinos. The closest reactors are the Bruce reactors, followed by the Pickering and Darlington reactors, whose baselines happen to match well the  $\Delta m^2$  to which Bruce is sensitive. Other, more distant reactors at various baselines contribute far less, and therefore SNO+ is in an excellent position to see the structure within the antineutrino spectrum that this nearly single-baseline provides. With those spectral effects, SNO+ has sensitivity to  $\Delta m^2$  similar to KamLAND, despite the much lower flux of reactor antineutrinos.

## V. CONCLUSIONS

SNO+ will provide a sensitive search for  $0\nu\beta\beta$  decay even in its initial 0.3% Te-loading phase, and also includes an interesting broad program of other physics measurements. The rapidly improving techniques developed by the SNO+ collaboration for the loading and purification of Te, the improvements to the optical properties with new wavelength shifters such as perylene, and the availability of high-quantum efficiency PMTs make the future of this approach particularly exciting. We look forward to the first demonstrations with SNO+ in its 0.3% Te phase, and the work ahead to push far beyond this.

### Acknowledgments

This work has been supported by the United States Department of Energy, Office of Nuclear Physics, the Science and Technology Facilities Council of the United Kingdom, the National Sciences and Engineering Research Council of Canada, the Canada Foundation for Innovation, the Canadian Institute for Advanced Research, the Fundação para a Ciência e a Tecnologia of Portugal, the Deutsche Forschungsgemeinschaft, and the European Union's Seventh Framework Programme ([FP7/2007-2013], under the European Research Council (ERC) grant agreement no. 278310 and the MarieCurie grant agreement no: [PIEF-GA-2009-253701])

- 
- [1] J. Barea, J. Kotila, F. Iachello, "Nuclear matrix elements for double-beta decay," *Phys. Rev. C* **87**, 014315 (2013).
  - [2] J. Kotila, F. Iachello, "Phase space factors for double-beta decay," *Phys. Rev. C* **85**, 034316 (2012).
  - [3] C. Arpesella *et al.*, *Phys. Rev. Lett.* **101**, 091302 (2008); J. Benziger *et al.*, *Nucl. Instrum. Meth. A* **587**, 277 (2008)
  - [4] V. Lozza and J. Petzoldt, "Cosmogenic activation of a natural tellurium target," *Astropart. Phys.* **61**, 62 (2015).
  - [5] J. J. Back, Y. A. Ramachers, *ACTIVIA: Calculation of isotope production cross-sections and yields* *Nucl. Instr. Meth. A* **586** (2008) 286-294
  - [6] T.W. Armstrong, K.C. Chandler, J. Barish, *J. Geophys. Res.* **78** (1973) 2715
  - [7] N. Gehrels, *Nucl. Instr. and Meth. A* **239** (1985) 324
  - [8] R. Silberberg, C.H. Tsao, *Astrophys. J. Suppl.* **220** (I) **25** (1973) 315; R. Silberberg, C.H. Tsao, *Astrophys. J. Suppl.* **220** (II) **25** (1973) 335
  - [9] R. Silberberg, C.H. Tsao, *Astrophys. J. Suppl.* **35** (1977) 129; R. Silberberg, C.H. Tsao, J.R. Letaw, *Astrophys. J. Suppl.* **58** (1985) 873; R. Silberberg, C.H. Tsao, J.R. Letaw, in: *Proceedings of the 20th International Cosmic Ray Conference*, Moscow, **2** (1987) 133; R. Silberberg, C.H. Tsao, *Phys. Rep.* **191** (1990) 351
  - [10] R. Silberberg, C.H. Tsao, A.F. Barghouty, *Astrophys. J.* **501** (1998) 911
  - [11] IDEA, *Upgrades in computational codes for studying cosmogenic activation in Double Beta Decay experiments* [http://idea.dipscfm.uninsubria.it/frontend/docs/reports/report\\_upgrade\\_codes.pdf](http://idea.dipscfm.uninsubria.it/frontend/docs/reports/report_upgrade_codes.pdf)
  - [12] The CUORE Collaboration, arXiv:1108.4757v2 [nucl-ex] (2011)
  - [13] A.J. Kaning and D. Rochman, TALYS-based Evaluated Data Library, <http://www.talys.eu>
  - [14] Bonventre, A. LaTorre, J.R. Klein, G.D. Orebi Gann, S. Seibert, O. Wasalski, "Non-Standard Models, Solar Neutrinos, and Large  $\theta_{13}$ ," *Phys. Rev. D* **88**, 053010 (2013).
  - [15] G. Bellini *et al.* [BOREXINO Collaboration], "Neutrinos from the primary proton-proton fusion process in the Sun," *Nature* **512**, no. 7515, 383 (2014).
  - [16] A. M. Serenelli, W. C. Haxton and C. Pena-Garay, "Solar models with accretion. I. Application to the solar abundance problem," *Astrophys. J.* **743**, 24 (2011)
  - [17] B. von Krosigk, L. Neumann, R. Nolte, S. Rottger and K. Zuber, "Measurement of the proton light response of various LAB based scintillators and its implication for supernova neutrino detection via neutrino-proton scattering," *Eur. Phys. J. C* **73**, 2390 (2013)
  - [18] T. Araki, et al. (KamLAND Collaboration), "Search for the Invisible Decay of Neutrons with KamLAND," *Phys. Rev. Lett.* **96**, 101802 (2006).